

**This is a self-archived version of an original article. This version may differ from the original in pagination and typographic details.**

**Author(s):** Spiliopoulos, Panagiotis; Gestranus, Marie; Zhang, Chao; Ghiyasi, Ramin; Tomko, John; Arstila, Kai; Putkonen, Matti; Hopkins, Patrick E.; Karppinen, Maarit; Tammelin, Tekla; Kontturi, Eero

**Title:** Cellulose-inorganic hybrids of strongly reduced thermal conductivity

**Year:** 2022

**Version:** Published version

**Copyright:** © 2022 Springer Nature B.V.

**Rights:** CC BY 4.0

**Rights url:** <https://creativecommons.org/licenses/by/4.0/>

**Please cite the original version:**

Spiliopoulos, P., Gestranus, M., Zhang, C., Ghiyasi, R., Tomko, J., Arstila, K., Putkonen, M., Hopkins, P. E., Karppinen, M., Tammelin, T., & Kontturi, E. (2022). Cellulose-inorganic hybrids of strongly reduced thermal conductivity. *Cellulose*, 29(15), 8151-8163.  
<https://doi.org/10.1007/s10570-022-04768-3>



# Cellulose-inorganic hybrids of strongly reduced thermal conductivity

Panagiotis Spiliopoulos · Marie Gestranus · Chao Zhang · Ramin Ghiyasi · John Tomko · Kai Arstila · Matti Putkonen · Patrick E. Hopkins · Maarit Karppinen · Tekla Tammelin · Eero Kontturi

Received: 27 January 2022 / Accepted: 17 July 2022  
© Springer Nature B.V. 2022

**Abstract** The employment of atomic layer deposition and spin coating techniques for preparing inorganic–organic hybrid multilayer structures of alternating ZnO–CNC layers was explored in this study. Helium ion microscopy and X-ray reflectivity showed the superlattice formation for the nanolaminate structures and atomic force microscopy established the efficient control of the CNCs surface coverage on the Al-doped ZnO by manipulating the concentration of the spin coating solution. Thickness characterization

of the hybrid structures was performed via both ellipsometry and X-ray reflectivity and the thermal conductivity was examined by time domain thermoreflectance technique. It appears that even the incorporation of a limited amount of CNCs between the ZnO laminates strongly suppresses the thermal conductivity. Even small, submonolayer amounts of CNCs worked as a more efficient insulating material than hydroquinone or cellulose nanofibers which have been employed in previous studies.

---

Panagiotis Spiliopoulos and Marie Gestranus have contributed equally to this work.

---

**Supplementary Information** The online version contains supplementary material available at <https://doi.org/10.1007/s10570-022-04768-3>.

---

P. Spiliopoulos · E. Kontturi (✉)  
Department of Bioproducts and Biosystems, Aalto University, P.O Box 16300, 00076 Aalto Espoo, Finland  
e-mail: eero.kontturi@aalto.fi

M. Gestranus · T. Tammelin  
VTT Technical Research Centre of Finland Ltd., P.O Box 1000, 02044 VTT Espoo, Finland  
e-mail: Tekla.Tammelin@vtt.fi

C. Zhang · M. Putkonen  
Department of Chemistry, University of Helsinki, P.O Box 55, 00014 Helsinki, Finland

R. Ghiyasi · M. Karppinen  
Department of Chemistry and Materials Science, Aalto University, 00076 Aalto Espoo, Finland

**Keywords** Cellulose nanocrystals · Zinc oxide · Hybrids · Thermal conductivity · Aluminum doping

J. Tomko · P. E. Hopkins  
Department of Materials Science and Engineering,  
University of Virginia, Charlottesville, VA 22904, USA

K. Arstila  
Department of Physics and Nanoscience Center, University of Jyväskylä, P.O Box 35, 40014 Jyväskylä, Finland

K. Arstila  
Nanoscience Center, University of Jyväskylä, P.O. Box 35, 40014 Jyväskylä, Finland

P. E. Hopkins  
Department of Mechanical and Aerospace Engineering,  
University of Virginia, Charlottesville, VA 22904, USA

P. E. Hopkins  
Department of Physics, University of Virginia,  
Charlottesville, VA 22904, USA

## Introduction

Hybrids of inorganic–organic materials are expected to hold a pivotal role in future research topics, since the structural idea beyond them focuses on combining the desired properties out of each component. Accounts on hybrid materials are prominent in the fields of, e.g., electrochemistry (Zoubi et al. 2020), sensors (Jiang et al. 2013; Kladsomboon et al. 2018) optoelectronic devices (Majee et al. 2015; Chung et al. 2011) and fuel cells (Nie et al. 2017). Organic layers sandwiched between inorganic layers can contribute to the harvesting of thermoelectric energy in thin film structures by decreasing the thermal conductivity of the material without negative influence on the electrical properties (Wan et al. 2015, 2017). Overall, the effect of organic layers on the reduction of the thermal conductivity of inorganic structures has been analytically explained (Krahl et al. 2018; Giri et al. 2016a, b; Liu et al. 2013). However, their efficient fabrication in a single pattern still exhibits a number of challenges. Inorganic thin film production by atomic layer deposition (ALD) has during recent decades developed into an industrial coating method, while still retaining its position as an indispensable method for deposition of thin inorganic layers in research context due to the numerous permutations of elements. Recently, the development in molecular layer deposition (MLD) and its combination with ALD has enabled the production of nanoscale organic–inorganic hybrid superlattices with molecular control over the layer thickness (Tynell et al. 2014; Khayyami et al. 2019). Alternating inorganic–organic superlattice thin films with strongly reduced thermal conductivity have previously also been made from larger organic particles, namely nanocellulose, in which alternating layers have been produced by ALD deposition of ZnO and dip coating (Jin et al. 2017). In this paper, we want to refine the approach further by combining ALD deposition of ZnO layers with spin coating of well-defined nanocellulose layers, to introduce efficiency and tunability that could not be achieved by the dip coating technique. To our knowledge, the combination of these two techniques to yield multilayer hybrid structures has not been reported so far.

As a semiconductor, ZnO possesses many positive attributes for thermoelectric energy harvesting, such as high electrical conductivity and high Seebeck

coefficient (Hahn et al. 1951). Moreover, ZnO is non-toxic, inexpensive and a commonly used material deposited with ALD, and its behavior is well known and predictable as it is considered an ALD prototype material (Tynell et al. 2014; Yousfi et al. 2000). The high thermal conductivity of ZnO is, however, a challenge in thermoelectric applications. Aluminum doping of ZnO has been introduced as a method to decrease the thermal conductivity of nanocomposites (Jood et al. 2011). As stated in the previous, also the introduction of organic materials with low thermal conductivity has been suggested to reduce it (Tynell et al. 2014; Jin et al. 2017).

Nanocellulose has been topical for the past 10–15 years in materials research that has capitalized on its advanced mechanical properties (Aitomäki et al. 2014), high surface area (Phanthong et al. 2018), low toxicity (Endes et al. 2016) and low thermal conductivity (Hori et al. 2005; Uetani et al. 2017; Wicklein et al. 2015) among others. In fact, the thermal stability of nanocellulose has been extensively studied via thermogravimetric (TG) techniques, exhibiting structural integrity up to 200 °C, (Lu et al. 2020; Zhang et al. 2018, 2019) rendering it as an excellent component in hybrid structures, suitable for mildly elevated temperatures (Chiang et al. 2020; Sadasivuni et al. 2016). Furthermore, energy related applications, such as supercapacitors (Zu et al. 2016; Jose et al. 2019) have gained ground. Inclusion of nanocellulose in thin film structures has been translated into solutions for sensors in particular (Mangayil et al. 2017; Nguyen et al. 2019). Increased focus has also been paid in constructing graphene/nanocellulose thin films as promising structures in energy related applications due to their intrinsic thermal stability and electrical properties (Yang et al. 2017; Pottathara et al. 2021; Nie et al. 2020a, b). Furthermore, Klochko et al. (2020) developed flexible thermoelectric thin films through the combination of copper iodide with nanocellulose. Overall, the incorporation of nanocellulose in an inorganic structure for efficient manipulation of the thermal properties in the final hybrid composite, has been analytically described (Nie et al. 2020a, b; Zhang et al. 2020, 2019). Previously, we have optimized the low temperature ALD multilayer deposition process on nanocellulose for the control over oxygen and water vapor transmission rates (Putkonen et al. 2017). The employment of

nanocellulose for fabrication of energy-related hybrid inorganic–organic systems, however, still exhibits plenty of space to be explored.

Nanocelluloses are categorized into two main types: CNFs are flexible, usually mechanically isolated microfibrils that gel easily in water (Kim et al. 2015), while CNCs refer to much shorter rigid, rod-like particles (Dufresne et al. 2019), isolated by acid hydrolysis (Pääkkönen et al. 2019; Chen et al. 2015). As a result, CNCs exhibit higher chemical homogeneity than CNFs because the hemicellulose with CNCs has been mostly degraded and removed upon the hydrolysis (Spiliopoulos et al. 2021; Wyman et al. 2005; Gao et al. 2014). In addition, their employment carries another significant advantage: CNCs can be coated as well-defined submonolayers and continuous films on metal oxide surfaces, with efficient control over the uniform surface coverage by simply altering the solution concentration in spin coating (Kontturi et al. 2007). Previous work by our group has focused on the ZnO thermal conductivity reduction by the incorporation of TEMPO oxidized cellulose nanofibers (TOCNFs) between the ZnO layers by dip coating of the substrates into a TOCNFs dispersion, resulting in hybrid superlattice structures with potential as possible thermoelectric materials (Jin et al. 2017). However, because the CNF coverage is difficult to control, the effect was not quantified to the organic/inorganic component ratio. In principle, dip coating by adsorption cannot guarantee reproducibility for the ZnO layer surface coverage with CNF, in contrast to spin coating CNCs, for which all the experimental parameters can be accurately controlled (Sahu et al. 2009).

In this study, a simple and easily reproducible experimental protocol was applied, aiming at the incorporation of cellulose nanocrystals (CNCs) between ZnO to construct hybrid nanolaminates. To investigate the efficiency of our protocol, we resorted to a sizeable variety of characterization techniques: helium ion microscopy (HIM) and X-ray reflectivity (XRR) for the superlattice structure, atomic force microscopy (AFM) for the layer morphology, ellipsometry and XRR for the layer thickness, and time domain thermoreflectance (TDTR) for thermal conductivity of the resulting ultrathin films. Figure 1 shows the construction of hybrid superlattice structures involving Al-doped ZnO nanolaminates

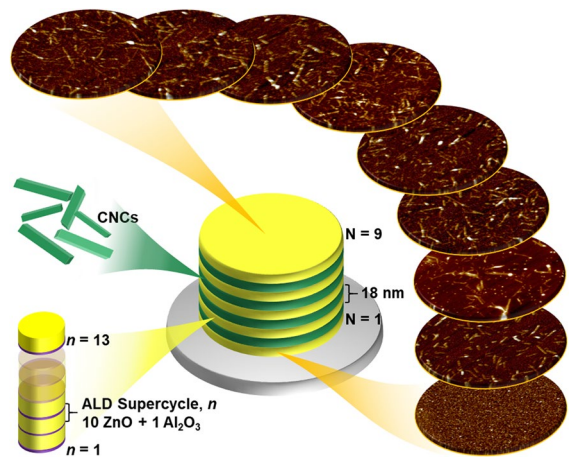


**Fig. 1** Hybrid superlattice thin film structure, consisting of 5 Al-doped ZnO layers alternating with 4 CNC layers. The AFM images on the outer ring represent collected images of each layer

interspaced with CNCs at different surface coverage. Organic and inorganic layers were prepared by spin coating and ALD, respectively. Spin coating is a fast and reproducible technique for cellulose films fabrication (Kontturi et al. 2003) whereas ALD is a well-established, efficient method for facilitating inorganic thin films, like ZnO in a highly conformal fashion (Singh et al. 2014; Boyadjiev et al. 2016). Herein, a significant reduction in thermal conductivity was demonstrated, even by the incorporation of very limited amounts of CNCs in the superlattice.

## Experimental

### CNC preparation

Commercial bacterial cellulose (BC, Chaokoh Nata De Coco, Theppadungporn Coconut Co., Ltd, Thailand) was used as the raw material of CNCs. The BC cubes were stored in coconut gel and washed thoroughly with pure water followed by alkali extraction with 0.1 M NaOH (3 h, 85 °C) for purification. Finally, the BC cubes were once more washed thoroughly with pure water. The extracted product was freeze dried (Edwards Micro Modulyo Freeze Dryer, Crawley, England) with the noted pre-treatments to dry matter content >90%. The HCl gas hydrolysis of the freeze-dried material down to LODP

(Leveling-off Degree of Polymerization) took place in a custom-built reactor (Pääkkönen et al. 2018) at 1.0 bar of pressure for 21 h, followed by degassing and extensive washing with milli-pore water. TEMPO-mediated oxidation was performed in a Büchi reactor (volume 1.6 dm<sup>3</sup>) as described by Pääkkönen et al. (2019) and the charge-carboxylate content of the hydrolyzed and TEMPO-oxidized BC was determined by conductometric titration (SCAN-CM 65:02) using Metrohm 751 GPD Titrino automatic titrator and Tiamo 1.2.1. Software. The charge content was calculated to 1.0 mmol/g, arising exclusively from the carboxylate amount of the sample. The average dimensions of the BC-CNCs were extracted from atomic force microscopy (AFM) and transmission electron microscopy (TEM) measurements and found to be 170 nm in length and 10 – 15 nm in diameter (Pääkkönen et al. 2019).

#### Hybrid inorganic–organic thin films preparation

The hybrid superlattice structures were fabricated by alternation of ALD depositions of Al-doped ZnO layers and spin coating of cellulose nanocrystals (CNCs) dispersions of three different concentrations: 25, 100 and 250 mg dm<sup>-3</sup>. Single side polished Si wafers of P-type doped with boron and with the orientation (100) produced by Okmetic were cut with a dicing saw (Disco Corporation, Tokyo, Japan) to 1 × 1 cm<sup>2</sup> substrates. Prior to use, the substrates were cleaned by soaking for 5 min in 2.5 M NaOH, followed by rinsing in Milli-Q water and drying with N<sub>2</sub> gas. The substrates were further coated with 5 layers of ZnO separated by 4 layers of CNCs (Fig. 1). The layered structures were additionally prepared on 1 × 1 cm<sup>2</sup> single-side polished sapphire substrates (AdValue Technology, Tucson), following exactly the same procedure. The process was repeated for all CNC concentrations. The ALD deposition of ZnO was performed at 90 °C in a Picosun™ R-200 reactor (Picosun Oy, Espoo, Finland). The operating pressure of the reaction chamber was around 10 mbar. Inert nitrogen gas with a purity of 99.999% was used as the carrier and purge gas. Diethyl zinc (DEZ, ≥ 52 wt. % Zn basis) purchased from Sigma-Aldrich) and distilled (DI) water were used as precursors for

the deposition of ZnO. The pulse time of 0.2 s and purge time of 7.0 s were used for both precursors. ZnO doping was carried out by Al<sub>2</sub>O<sub>3</sub> via the use of trimethyl aluminum (TMA) and H<sub>2</sub>O as precursors with the pulse and purge times of 0.3 and 10.0 s for both precursors. The growth rates of binary materials for ZnO and Al<sub>2</sub>O<sub>3</sub> thin films were around 0.2 nm/cycle and 0.1 nm/cycle, respectively. Al doping content in ZnO films was controlled by the so-called supercycle ALD, i.e., a single TMA-H<sub>2</sub>O cycle was inserted after a defined number of DEZ-H<sub>2</sub>O water cycles (Banerjee et al. 2010). The ALD supercycle of 13 × [10 × (DEZ + H<sub>2</sub>O) + 1 × (TMA + H<sub>2</sub>O)] was used to deposit the ZnO thin films with a target thickness of around 20 nm and the estimated Al doping ratio of 5%. Notably, in order to attain a uniform growth of ZnO thin films on the nanocellulose coating, 3 cycles of TMA-H<sub>2</sub>O ALD were conducted before the ZnO ALD supercycles, as proposed by Baji et al. (2012). Spin coating of CNCs took place via a P-6000 spin coater (Speedline Technologies, Inc.) at 4,000 rpm for 90 s.

#### Helium ion microscopy (HIM)

For HIM imaging of the thin film hybrid structures, reference samples of tin on carbon and gold on silicon were employed. The hybrid films were placed on 45° stubs and imaged from flat cleaved edge and from a scratch through a diamond pen. The imaging was performed via a Carl Zeiss Orion NanoFab instrument, utilizing a 35 keV helium beam. The working distance varied between 7–8 mm and the sample position alternated between 45° and 90° relative to the beam. The beam current was 0.15 – 0.20 pA and the image size 2048 × 2048 pixels. The dwell time was set at 10.0 μs and the line averaging at 4. Charge neutralization (flood gun) was not used. The pressure in the measurement chamber was 1.7 × 10<sup>-7</sup> Torr. Finally, all images were post-processed by level adjustment and gamma.

#### Atomic force microscopy (AFM)

The hybrid films were examined after each coating layer by an AFM Multimode 8 microscope (J scanner) from Bruker AXS Inc. (Madison, Wisconsin)

USA) for all concentrations of CNCs. The imaging was done with Ultrasharp  $\mu$ masch silicon tips (HQ: NSC15/Al BS, Tallin, Estonia) via tapping mode. The typical force constant was 40 N/m and the resonance frequency was 325 kHz. Third order flattening and 3D image generation was performed in Nanoscope Analysis 1.5 software. The analysis of film images and the surface coverage estimation were subsequently done by ImageJ 1.52a (Wayne Rasband, National Institute of Health, USA) software.

#### Ellipsometry characterization

Hybrid films thickness values were measured by a FS-1 multiwavelength ellipsometer (Film Sense), after each ZnO coating layer. Wavelengths of 465, 525, 590 and 635 nm were used to acquire the data. The Cauchy model was used for modeling the optical constants of the ZnO films.

#### X-Ray reflectivity (XRR)

The multilayer superlattice formation was analyzed by an X'pert Reflectivity v. 1.3 from PANalytical. The patterns were fitted by structural modelling. For the hybrid superlattice films, the initial fitting model – from bottom to top, respectively – included the following layers: Si substrate, SiO<sub>2</sub>, ZnO layer (10% Al<sub>2</sub>O<sub>3</sub>), corresponding number of cellulose and ZnO (10% Al<sub>2</sub>O<sub>3</sub>) layers, ending up with Al<sub>2</sub>O<sub>3</sub> and (H<sub>2</sub>O + CO<sub>2</sub>) on top. The experimental data were fitted using Reflex v44 (Vignaud et al. 2019). During the fitting process all parameters including thickness, density and roughness as well as instrumental factors were adjusted for fitting to the experimental pattern. The thickness values were confirmed by Fourier method to improve their reliability. Analytical details on the fitting procedure are described in the Supplementary Information (S3).

#### Time-domain thermoreflectance (TDTR)

The cross-plane thermal conductivity of the hybrid films was determined with the time-domain thermoreflectance (TDTR) technique at room temperature. Hybrid films of 5 inorganic (ZnO) and 4 organic (CNCs) layers were prepared on sapphire substrates and employed for the measurements. The thermal conductivity of the samples was obtained by fitting

of the experimental ‘cooling curve’ with a multilayer heat flow model (Cahil et al. 2004), where the thermo physical properties of the substrate and a metal transducer layer (80 nm Al), as well as the thermal resistance of their respective interfaces, are accounted for. In principle, the heat flow model takes under consideration: (i) an Al film transducer (necessary for TDTR measurements to relate the measured reflectivity to temperature), (ii) the ZnO/CNC hybrid film, (iii) the sapphire substrate. The pertinent details of the experimental setup and the analysis procedure to determine the thermal conductivity of the hybrid thin films can be found by Giri et al. (2016a, b).

## Results and discussion

The formation of a superlattice structure was confirmed using several different methods. Figure 2 shows the HIM images visualizing the multilayered (N=9) hybrid structure of the sample cross sections. The use of HIM allowed images clearly showing the inorganic–organic layer alteration, making it evident that the formation of ZnO/CNC hybrid layered structures had been successful.

Alongside the HIM images, a clear sign of the superlattice structure was provided by the XRR data, strengthening the validity of the concept. The alternation of the superlattice peaks as the coating procedure is advancing is clearly visible through the reflection pattern of Fig. 3. The formation of the regular superlattice structure is seen from the appearance of regularly repeating more intense peaks in the patterns. Such superlattice peaks are absent for single-layer ZnO film. Then, when the number of repeating layers increase, also the number of the smaller peaks in between two consequent superlattice peaks systematically increases, as shown in previously published hybrid multilayer systems (Krahl et al. 2020; Jin et al. 2017).

The formation of additional intermediate fringes (denoted by red arrows) between the superlattice peaks (denoted by blue arrows) is notable as the N number is increasing from 3 to 9 (Fig. 3). This is independent of the CNC concentration and hence attributed exclusively to the formation of additional layers, in agreement with previous reports (Jin et al. 2017; Ha et al. 2011), as a result of the different electron densities between the organic and the inorganic

**Fig. 2** HIM images of the cross sections of **a** ZnO/CNC ( $N=9$ ,  $c=25 \text{ mg dm}^{-3}$ ), **b** ZnO/CNC ( $N=9$ ,  $c=100 \text{ mg dm}^{-3}$ ), **c** ZnO/CNC ( $N=9$ ,  $c=250 \text{ mg dm}^{-3}$ ) and **d** ZnO/CNC ( $N=9$ ,  $c=100 \text{ mg dm}^{-3}$ )

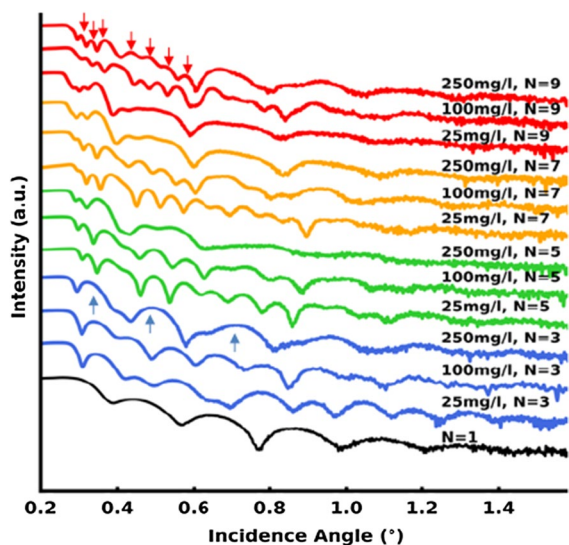
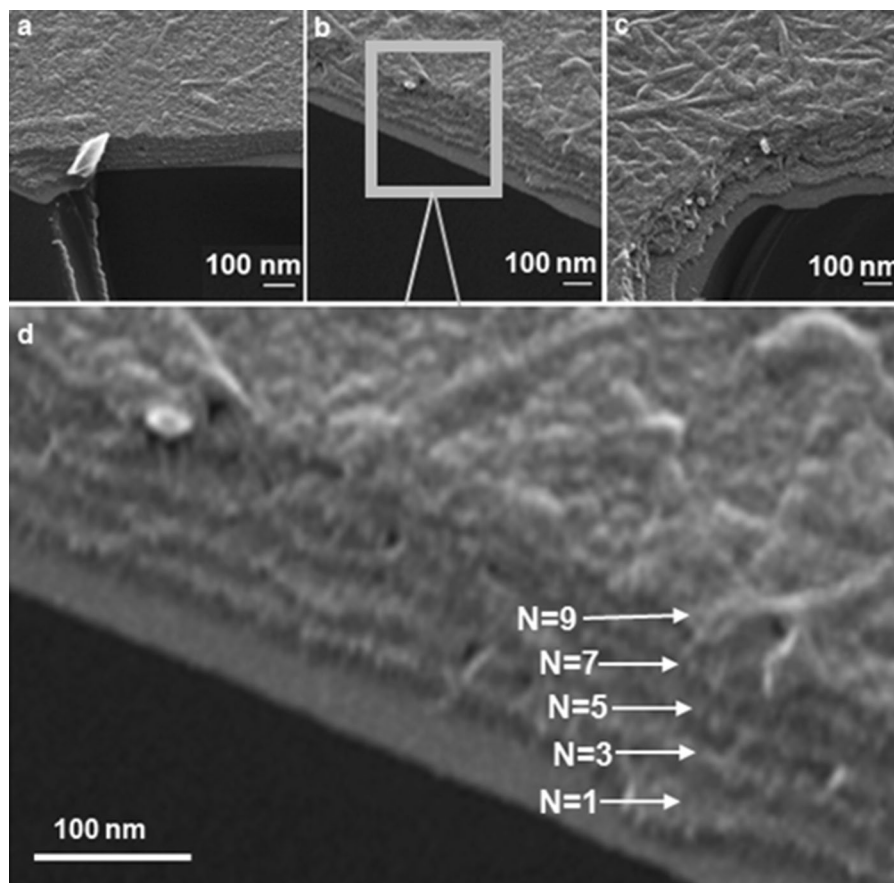


**Fig. 3** XRR patterns of the hybrid samples. N number denotes the coating layer sequence and each concentration is mentioned above the corresponding pattern. The red arrows point to the emerging intermediate fringes and the blue arrows to the superlattice peaks, growing more prominent with increasing N

component. For the  $250 \text{ mg dm}^{-3}$  concentration hybrids these fringes appear broader throughout all the (N) layers, something that could be attributed to the full coverage provided by the CNC layers on the ZnO (see, Fig. 4 – AFM analysis and Table 1).

The CNC surface coverage for the ZnO/CNC ( $N=2$ ,  $c=25 \text{ mg dm}^{-3}$ ) and ZnO/CNC ( $N=2$ ,  $c=100 \text{ mg dm}^{-3}$ ) was extracted through ImageJ software analysis. However, the results for the ZnO ( $N=2$ ,  $c=250 \text{ mg dm}^{-3}$ ) were misleading. Increase of the concentration to  $250 \text{ mg dm}^{-3}$  provides full CNC coverage on the ZnO wafer, yet ImageJ analysis was unable to establish it due to the inability of detecting the CNCs underneath the top layer. Therefore, we present the corresponding phase contrast images to demonstrate the full-coverage for the  $250 \text{ mg dm}^{-3}$  CNC layer (Fig. 4). The lower concentrations show clear phase contrast between the substrate and the CNCs (Figs. 4a and 4b) whereas the CNC layer spin coated from  $250 \text{ mg dm}^{-3}$  concentration shows a

**Fig. 4** Phase contrast AFM images of the N=2 hybrids for the three different concentrations employed

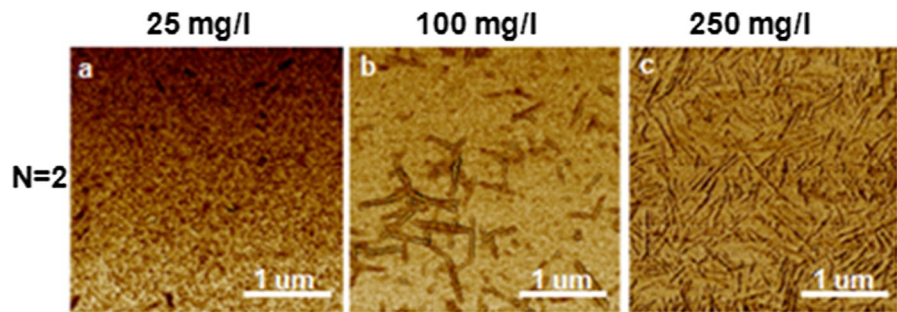


**Table 1** Surface coverage (SC) values and roughness (root mean square) values for the ZnO/CNC (N=2, c=25 mg dm<sup>-3</sup>), ZnO/CNC (N=2, c=100 mg dm<sup>-3</sup>) and ZnO/CNC (N=2, c=250 mg dm<sup>-3</sup>) hybrids, as calculated by image analysis from AFM data

ZnO/CNC sample	N=2, c=25 mg dm <sup>-3</sup>	N=2, c=100 mg dm <sup>-3</sup>	N=2, c=250 mg dm <sup>-3</sup>
CNC, SC %	12.3 ± 2.08	17.3 ± 0.57	100
Roughness (nm)	3.0	3.5	3.3

uniform phase (Fig. 4c), indicating that the layer is made of a single material only.

In principle, the intercalating full-coverage CNC layers between the inorganic ones result in efficient separation of the superlattice peaks, while the presence of lower coverage CNC layers (25 and 100 mg dm<sup>-3</sup>) appears not to lead to efficient ZnO layer separation. As a result, the XRR patterns from the films with 25 and 100 mg dm<sup>-3</sup> CNC concentrations appear not as distinct as those from the films with 250 mg dm<sup>-3</sup> CNC concentration. This occurs simply because the ZnO/CNC interfaces for the 25 and 100 mg dm<sup>-3</sup> hybrid films are not perfectly defined, due to the lower coverage at the smaller CNC concentrations – an explanation which is also supported by our previous study (Jin et al. 2017).

The Si-wafers substrates were efficiently coated with Al-doped ZnO (N=1) whose morphology and surface coverage is demonstrated in the Supplementary Information (Fig. S1). For the following layers, AFM height images after layers N=2, 3, 9 are presented in Fig. 5 and corresponding AFM height images for the remaining deposition steps are available in the Supplementary Information (Fig. S2).

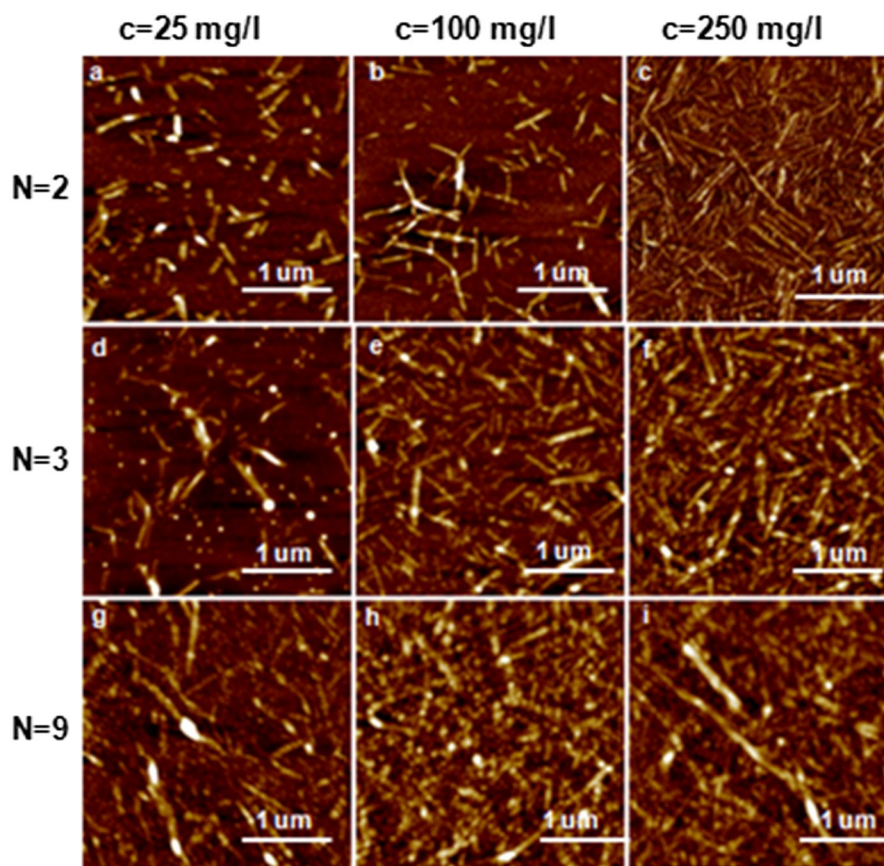
The ZnO deposition on CNCs induces a morphological alteration especially on ZnO/CNC (N=3, c=25 mg dm<sup>-3</sup>) and ZnO/CNC (N=9, c=25 mg dm<sup>-3</sup>) films, as well as through the intermediate stages (see also Supplementary Information

Fig. S2) where the consecutive coating layers result in visible roughness increase in the AFM images. In fact, the lower CNC coverage of ZnO/CNC (N=2, c=25 mg dm<sup>-3</sup>) and ZnO/CNC (N=2, c=100 mg dm<sup>-3</sup>) enables the visualization of the coating effect via comparison with the ZnO/CNC (N=9, c=25 mg dm<sup>-3</sup>) and ZnO/CNC (N=9, c=100 mg dm<sup>-3</sup>) images. It should also be mentioned that the lower roughness indicated for the 25 mg/l concentration hybrids from the XRR analysis (Fig. 3), appears to be beneficial for observing the coating effect through the AFM images, in contrast with the increased roughness indicated for the 250 mg/l hybrids. Here, we emphasize the suitability of CNCs as the intercalating layer between the ZnO. CNCs provide a surface with an abundance of OH groups, which supports the formation of a ZnO layer due to their reactivity with the precursors molecules during ALD. The selection of another cellulose derivative with high degrees of substitution, e.g., cellulose xanthate (Weißl et al. 2019), would prohibit the formation of an efficient ALD coating because of a relatively low number of available OH groups. In total, the HIM, XRR and AFM measurements have provided us with a clear evidence of the concept on the hybrid multilayered structure formation.

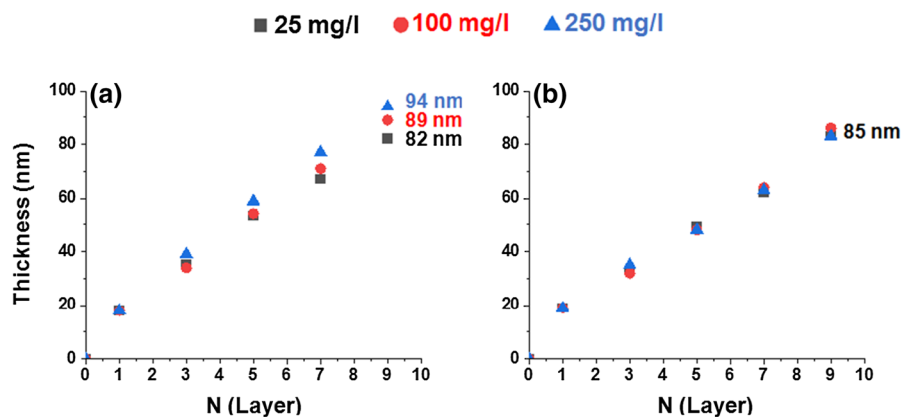
Ellipsometry measurements took place after every ZnO deposition to establish the thickness values of



**Fig. 5** AFM height images of the hybrid samples. The coating layer number ( $N$ ) and the concentration  $c$  are denoted for every sample



**Fig. 6** Thickness values of the hybrid samples extracted from **a** Ellipsometry and **b** XRR characterization for all the ZnO/CNC hybrids



the hybrids. Figure 6 shows these values, together with those from the XRR characterization, demonstrating a good correlation between the two techniques for thickness measurements.

As expected, the addition of layers increases the overall hybrid film thickness linearly with the number of layers added. Additionally, a small effect of

the CNC concentration on the overall hybrid film thickness was detected by ellipsometry in Fig. 6a, as higher CNC concentrations resulted into thicker films. The XRR data did not detect these small variations in the total film thickness caused by the CNC concentration, probably due to the film roughness (Table 1), so only an average value of 85 nm for  $N=9$

**Table 2** Thickness values for the ZnO/CNC (N=9, c=25 mg dm<sup>-3</sup>), ZnO/CNC (N=9, c=100 mg dm<sup>-3</sup>) and ZnO/CNC (N=9, c=250 mg dm<sup>-3</sup>) hybrids, as calculated by image analysis from three different points from the HIM data

Sample	Thickness (nm)			Average
	p1	p2	p3	
N=9 c=25 mg dm <sup>-3</sup>	76.2	72.9	75.3	74.8
N=9 100 mg dm <sup>-3</sup>	80.7	81.6	82.3	81.5
N=9 250 mg dm <sup>-3</sup>	88.8	89.0	93.2	90.3

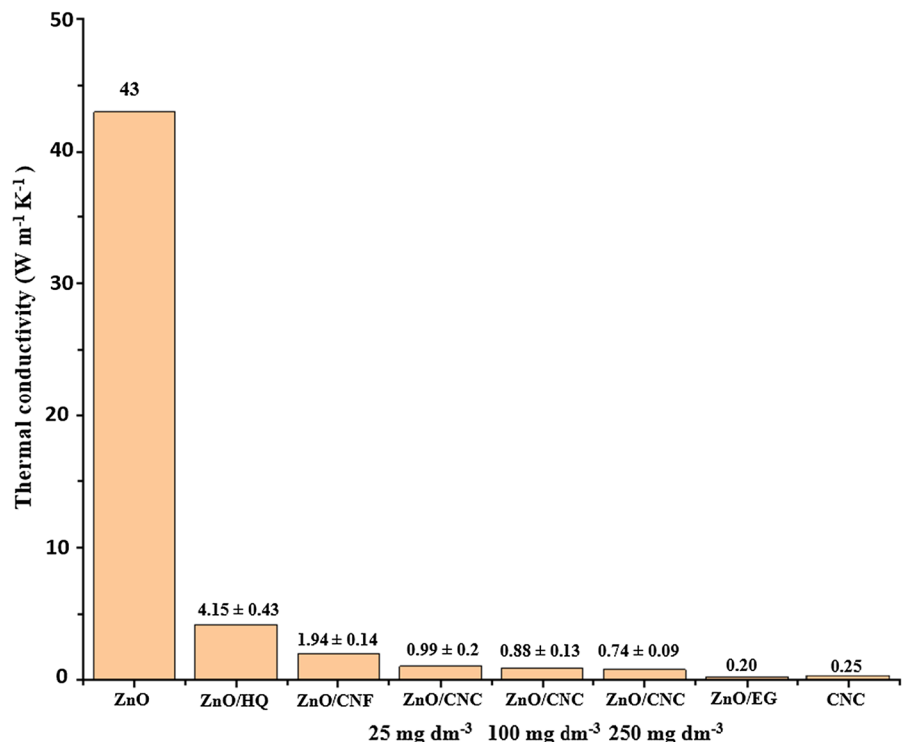
CNC/ZnO samples is presented in Fig. 6b. On the other hand, the XRR data enabled us to determine the individual CNC layer thicknesses in the hybrid films: this value was found to increase from 1.5 nm to 3.0 nm and finally to 3.5 nm with increasing CNC concentration from 25 to 100 and to 250 mg dm<sup>-3</sup> respectively. Thickness measured by XRR and ellipsometry also corresponds relatively well to thickness measurement from the HIM images as well, as presented in the Table 2. Image analysis from HIM images gave slightly smaller thickness estimates, in

the range of -4 to -7 nm compared to ellipsometry, possibly due to the ultra-high vacuum the samples were subjected to in the HIM. The minor variations in thickness – measured from several different locations of the N=9 hybrids with HIM – underline a uniform thickness throughout the sample and the repeatability of the layer build up process.

Comparing the thickness of the (ZnO/CNC, N=9) hybrids with the ZnO/CNF from Jin et al. (2017) small variations were detected. Especially for the 100 mg/l CNC concentration the thickness of 94 nm provided from the ellipsometry data, is very close to the approximation of 100 nm for the ZnO/CNF N=9, but the comparison between CNC and CNF layers between these two studies should be treated with caution because of the completely different premises of the coating techniques.

The thermal conductivity values obtained from the TDTR measurements are demonstrated in Fig. 7. The entire N=9 samples for 25, 100 and 250 mg dm<sup>-3</sup> CNC concentrations were examined and a comparison to ZnO-based hybrid samples of different organic components (hydroquinone, cellulose nanofibers, ethylene glycol (EG) and CNCs itself from previous studies (Tynell et al. 2014; Jin et al. 2017; Liu et al.

**Fig. 7** Thermal conductivity values measured for the ZnO/CNC, N=9 hybrid samples (red frame) compared with results of previous studies (Tynell et al. 2014; Jin et al. 2017; Lui et al. 2013). Thermal conductivity of pristine CNC layer was retrieved from Diaz et al. (2014)



2013; Diaz et al. 2014) is presented. A large reduction in the thermal conductivity takes place for all the ZnO/CNC samples not only compared to that of a ZnO film (Alvarez-Quintana et al. 2010) but also to the values of other hybrid systems.

Cellulose nanofibers (CNF) have been proved more efficient in reducing the thermal transport in ZnO films (Jin et al. 2017) than hydroquinone (HQ), but the incorporation of CNC layers between the ZnO laminates resulted in even lower thermal conductivity, as demonstrated in Fig. 6. Herein, the comparison between the thermal conductivities of ZnO/CNF and ZnO/CNC hybrids is relevant since all of them are composed of the same layer number ( $N=9$ ). The ALD layers produced in this study are doped with aluminum, which is a known route to reduce the thermal conductivity of ZnO in bulk when compared to ZnO and  $\text{ZnAl}_2\text{O}_4$  nanocomposites (Jood et al. 2011). However, the system differs highly from the one in this study, as it is disordered compared to this nanolaminate. It is also clear that the incorporation of different CNC concentrations affects the thermal conductivity value. We attribute this to the increasing CNC layer thickness (1.5, 3.0 and 3.5 nm) with increasing CNC concentration (25, 100 and  $250 \text{ mg dm}^{-3}$ ), in agreement with the previous studies (Jin et al. 2017; Ghiyasi et al. 2020, 2021) which have also pointed out the beneficial role of the increased organic layer thickness in depressing the thermal conductivity of the hybrid. However, despite the unequivocal effect of the CNC incorporation on the ZnO thermal conductivity, more efficient thermally insulating systems have been reported, e.g., ZnO/EG (Liu et al. 2013), which was even lower than the thermal conductivity of plain CNCs (Diaz et al. 2014). The mechanism of the thermal conductivity reduction is based on blocking the phonons, responsible for heat transmittance, by the incorporation of organic layers with poor thermal conductivity between the ZnO laminates. However, the specific structural details leading to quantitative differences in reduced thermal conductivity by the organic layers in hybrid systems have not been elucidated. One of the future tasks is to develop a theoretical framework around the mechanism of thermal conductivity reduction in hybrid multilayer systems. This will enable tools for optimization but it is outside the scope of the current, descriptive study.

It is apparent that the technique of spin coating in this work facilitates defined cellulose layers in a more

reproducible and accurate manner than the simple dipping of the substrate in the CNF suspension that was performed by Jin et al. (2017), as it allows a more efficient control of the coating parameters (spinning speed and time). As a result, homogeneously spread layers of CNCs lead to a more efficient scattering of phonons, thereby minimizing the cross-plane thermal conduction. It would be reasonable to assume that increasing the CNC concentration – and as a result the CNC surface coverage and finally the thickness of the organic component – would diminish the phonon propagation even further, but this was not the case. In fact, an increase of the CNC concentration (i.e., the thickness of the CNC layers) has a relatively mild effect on the thermal conductivity as an increase in concentration to 100 and  $250 \text{ mg dm}^{-3}$  reduced the thermal conductivity 11% and 25% respectively compared with the  $25 \text{ mg dm}^{-3}$  case. It appears that even the incorporation of a limited amount of CNCs through the ZnO laminates can induce a significant reduction in the thermal conductivity, while the formation of a full-coverage CNC layer is not a requirement for achieving this reduction.

## Conclusions

Layered hybrid ZnO/CNC films were prepared by a combination of ALD and spin coating techniques. HIM, XRR and AFM data confirmed the presence of a multilayered structure, constructed of discrete, alternating layers of ZnO and CNC, amounting to superlattice structures. TDTR examined the hybrids cross plane thermal conductivity, establishing a large reduction after the CNC incorporation. It appears that even the formation of a CNC submonolayer, without ensuring full coverage on the ZnO wafers, can result in efficient phonons scattering through the cross plane, while the intercalation of thicker CNC layers causes a mild additional decrease in the thermal conductivity of the hybrid film.

**Acknowledgments** PS and MG would like to acknowledge Academy of Finland (grants no. 300364 and 300367) for the financial support. MK and RG would like to acknowledge the European Union's Horizon 2020 research and innovation program under the Marie Skłodowska-Curie grant agreement (No. 765378), Academy of Finland (Profi 3) and the use of Raw-Matters Finland Infrastructure (RAMI) at Aalto University. M.P acknowledges funding from Academy of Finland by the

profiling action on Matter and Materials, grant no. 318913. The work is a part of FinnCERES Materials Bioeconomy Ecosystem. The use of ALD center Finland research infrastructure is acknowledged. PEH and JT acknowledge funding from the US Department of Defense, Multidisciplinary University Research Initiative through the Army Research Office, Grant no. W911NF-16-1-0406.

**Authors' contributions** Not applicable.

**Funding** Open Access funding provided by Aalto University. PS and MG were funded by Academy of Finland (grants no. 300364 and 300367). MK and RG received funding from European Union's Horizon 2020 research and innovation program under the Marie Skłodowska-Curie grant agreement (No. 765378), the Academy of Finland (Profi 3) and the use of RawMatters Finland Infrastructure (RAMI) at Aalto University. M.P received funding from the Academy of Finland by the profiling action on Matter and Materials, grant no. 318913. The work is a part of FinnCERES Materials Bioeconomy Ecosystem. PEH and JT received funding from the US Department of Defense, Multidisciplinary University Research Initiative through the Army Research Office, Grant no. W911NF-16-1-0406.

**Data Availability** Not applicable.

**Declarations**

**Conflict of interest** Not applicable.

**Consent to participate** All authors have participated in the writing of the manuscript and given their consent to submit the manuscript.

**Consent for publication** All authors consent to the publication of the manuscript.

**Ethics approval** There are no ethical issues to consider.

**Human or animal rights** Not applicable.

**Open Access** This article is licensed under a Creative Commons Attribution 4.0 International License, which permits use, sharing, adaptation, distribution and reproduction in any medium or format, as long as you give appropriate credit to the original author(s) and the source, provide a link to the Creative Commons licence, and indicate if changes were made. The images or other third party material in this article are included in the article's Creative Commons licence, unless indicated otherwise in a credit line to the material. If material is not included in the article's Creative Commons licence and your intended use is not permitted by statutory regulation or exceeds the permitted use, you will need to obtain permission directly from the copyright holder. To view a copy of this licence, visit <http://creativecommons.org/licenses/by/4.0/>.

## References

- Aitomäki Y, Oksman K (2014) Reinforcing efficiency of nanocellulose in polymers. *React Funct Polym* 85:151–156. <https://doi.org/10.1016/j.reactfunctpolym.2014.08.010>
- Alvarez-Quintana J, Martinez E, Pérez-Tijerina E, Pérez-García SA, Rodríguez-Viejo J (2010) Temperature dependent thermal conductivity of polycrystalline ZnO films. *J Appl Phys* 107:063713. <https://doi.org/10.1063/1.3330755>
- Baji Z, Lábadi Z, Horváth ZE et al (2012) Nucleation and growth modes of ALD ZnO. *Cryst Growth Des* 12:5615–5620. <https://doi.org/10.1021/cg301129v>
- Banerjee P, Lee WJ, Bae KR, Lee SB, Rubloff GW (2010) Structural, electrical, and optical properties of atomic layer deposition Al-doped ZnO films. *J Appl Phys* 108:043504. <https://doi.org/10.1063/1.3466987>
- Boydjiev SI, Georgieva V, Yordanov R, Raicheva Z, Szilágyi IM (2016) Preparation and characterization of ALD deposited ZnO thin films studied for gas sensors. *Appl Surf Sci* 387:1230–1235. <https://doi.org/10.1016/j.apsusc.2016.06.007>
- Cahill DG (2004) Analysis of heat flow in layered structures for time-domain thermoreflectance. *Rev Sci Instrum* 75:5119–5122. <https://doi.org/10.1063/1.1819431>
- Chen L, Wang Q, Hirth K, Baez K, Argarwal UP, Zhu JY (2015) Tailoring the yield and characteristics of wood cellulose nanocrystals (CNC) using concentrated acid hydrolysis. *Cellulose* 22:1753–1762. <https://doi.org/10.1007/s10570-015-0615-1>
- Chiang CH, Li TY, Wu SH et al (2020) High-stability inorganic perovskite quantum dot–cellulose nanocrystal hybrid films. *Nanotechnology* 31:324002. <https://doi.org/10.1088/1361-6528/ab8c79>
- Chung MH, Lin SJ, Hsieh TE, Chen NP, Juang FS, Chen SM, Liu LC (2011) Preparation of organic/inorganic hybrid nanocomposites by ultraviolet irradiation and their packaging applications for organic optoelectronic devices. *Appl Surf Sci* 257:9142–9151. <https://doi.org/10.1016/j.apsusc.2011.05.117>
- Diaz JA, Ye Z, Wu X, Moore AL, Moon RJ, Martini A, Boday DJ, Youngblood JP (2014) Thermal conductivity in nanostructured films: from single cellulose nanocrystals to bulk films. *Biomacromol* 15:4096–4101. <https://doi.org/10.1021/bm501131a>
- Dufresne A (2019) Nanocellulose processing properties and potential applications. *Curr Rep* 5:76–89. <https://doi.org/10.1007/s40725-019-00088-1>
- Endes C, Camarero-Espinosa S, Mueller S et al (2016) A critical review of the current knowledge regarding the biological impact of nanocellulose. *J Nanobiotechnology* 14:1–14. <https://doi.org/10.1186/s12951-016-0230-9>
- Gao X, Rajeev K, Wyman CE (2014) Fast hemicellulose quantification via a simple one-step acid hydrolysis. *Biotechnol Bioeng* 111:1088–1096. <https://doi.org/10.1002/bit.25174>
- Ghiyasi R, Girish CT, Karppinen M (2020) Organic-Component Dependent Crystal Orientation and Electrical Transport Properties in ALD/MLD Grown ZnO–Organic Superlattices. *J Phys Chem C* 124:13765–13770. <https://doi.org/10.1021/acs.jpcc.0c03053>

- Ghiyasi R, Milich M, Tomko J, Hopkins PE, Karppinen M (2021) Organic component dependent thermal conductivity reduction in ALD/MLD grown ZnO: organic superlattice thin films. *Appl Phys Lett* 118:211903. <https://doi.org/10.1063/5.0052450>
- Giri A, Niemelä JP, Szejkiowski CJ, Karppinen M, Hopkins PE (2016a) Reduction in thermal conductivity and tunable heat capacity of inorganic/organic hybrid superlattices. *Phys Rev B* 93:115–310. <https://doi.org/10.1103/PhysRevB.93.115310>
- Giri A, Niemelä JP, Tynell T, Gaskins JT, Donovan BF, Karppinen M, Hopkins PE (2016b) Heat-transport mechanisms in molecular building blocks of inorganic/organic hybrid superlattices. *Phys Rev B* 93:115310. <https://doi.org/10.1103/PhysRevB.93.115310>
- Ha YG, Emery JD, Bedzyk JM, Usta H, Facchetti A, Marks TJ (2011) Solution-Deposited Organic-Inorganic Hybrid Multilayer Gate Dielectrics. Design, Synthesis, Microstructures, and Electrical Properties with Thin-Film Transistors. *J Am Chem Soc* 133:10239–10250. <https://doi.org/10.1021/ja202755x>
- Hahn EE (1951) Some electrical properties of zinc oxide semiconductor. *J Appl Phys* 22:855–863. <https://doi.org/10.1063/1.1700063>
- Hori R, Wada M (2005) The thermal expansion of wood cellulose crystals. *Cellulose* 12:479–484. <https://doi.org/10.1007/s10570-005-5967-5>
- Jiang T, Wang Z, Li Z, Wang W, Xu X, Liu X, Wang J, Wang C (2013) Synergic effect within n-type inorganic–p-type organic nano-hybrids in gas sensors. *J Mater Chem C* 1:3017–3025. <https://doi.org/10.1039/C3TC00370A>
- Jin H, Marin G, Giri A, Tynell T, Gestranus M, Wilson BP, Kontturi E, Tammelin T, Hopkins PE, Karppinen M (2017) Strongly reduced thermal conductivity in hybrid ZnO/nanocellulose thin films. *J Mater Chem* 52:6093–6099. <https://doi.org/10.1007/s10853-017-0848-5>
- Jood P, Mehta RJ, Zhang Y et al (2011) Al-doped zinc oxide nanocomposites with enhanced thermoelectric properties. *ACS Nano* 11:4337–4342. <https://doi.org/10.1021/nl202439h>
- Jose J, Thomas V, Vinod V, Abraham R, Abraham S (2019) Nanocellulose based functional materials for supercapacitor applications. *J Sci Adv Mater Dev* 4:333–340. <https://doi.org/10.1016/j.jsamd.2019.06.003>
- Khayyami A, Philip A, Karppinen M (2019) Atomic/Molecular layer deposited iron–azobenzene framework thin films or stimuli-induced gas molecule capture/release. *Angew Chem Int Ed* 58:13400–13404. <https://doi.org/10.1002/anie.201908164>
- Kim JH, Shim BS, Kim SH et al (2015) Review of nanocellulose for sustainable future materials. *Int J Precis Eng Manuf* 2:197–213. <https://doi.org/10.1007/s40684-015-0024-9>
- Kladsomboon S, Thippakorn C, Seesaard T (2018) Development of Organic-Inorganic Hybrid Optical Gas Sensors for the Non-Invasive Monitoring of Pathogenic Bacteria. *Sensors* 18:3189. <https://doi.org/10.3390/s18103189>
- Klochko NP, Barbash VA, Klepikova KS, Kopach VR, Tyukhov II, Yashchenko OV, Zhadan TO, Petrusenko SI, Dukarov SV, Lyubov MA, Khrypunova AL (2020) Use of biomass for a development of nanocellulose-based biodegradable flexible thin film thermoelectric material. *Sol Energy* 201:21–27. <https://doi.org/10.1016/j.solener.2020.02.091>
- Kontturi E, Thüne PC, Niemantsverdriet JW (2003) Novel method for preparing cellulose model surfaces by spin coating. *Polymer* 44:3621–3625
- Kontturi E, Johansson LS, Kontturi KS, Ahonen P, Thüne PC, Laine J (2007) Cellulose nanocrystal submonolayers by spin coating. *Langmuir* 23:9674–9680. <https://doi.org/10.1021/la701262x>
- Krahl F, Giri A, Tomko JA, Tynell T, Hopkins PE, Karppinen M (2018) *Adv Mater Interfaces* 5:1701692
- Krahl F, Ge Y, Karppinen M (2020) Characterization of ZnO/AlOx/benzene thin-film heterostructures grown through atomic layer deposition/molecular layer deposition. *Semicond Sci Technol* 36:025012. <https://doi.org/10.1088/1361-6641/abcee2>
- Liu J, Yoon B, Kuhlmann E, Tian M, Zhu J, George MS, Lee CU, Yang R (2013) Ultralow thermal conductivity of atomic/molecular layer-deposited hybrid organic–inorganic zinc oxide thin films. *Nano Lett* 11:5594–5599. <https://doi.org/10.1021/nl403244s>
- Lu Y, TaO P, Zhang N, Nie S (2020) Preparation and thermal stability evaluation of cellulose nanofibrils from bagasse pulp with differing hemicelluloses contents. *Carbohydr Polym* 245:116463. <https://doi.org/10.1016/j.carbpol.2020.116463>
- Majee S, Cerqueira MF, Tondelier D, Geffroy B, Bonnasieux Y, Alpuim P, Bourée JE (2015) Flexible organic–inorganic hybrid layer encapsulation for organic optoelectronic devices. *Prog Org Coat* 80:27–32. <https://doi.org/10.1016/j.porgcoat.2014.11.015>
- Mangayil R, Rajala S, Pammo A, Sarlin E, Luo J, Santala V, Karp M, Tuukkanen S (2017) Engineering and characterization of bacterial nanocellulose films as low cost and flexible sensor material. *ACS Appl Mater Interfaces* 9:19048–19056. <https://doi.org/10.1021/acsami.7b04927>
- Nguyen LH, Naficy S, Chandrawati R, Dehghani F (2019) Nanocellulose for sensing applications. *Adv Mater Interfaces* 6:1900424. <https://doi.org/10.1002/admi.201900424>
- Nie Y, Gao J, Wang E, Jiang L, An L, Wang X (2017) An effective hybrid organic/inorganic inhibitor for alkaline aluminum–air fuel cells. *Electrochim Acta* 248:478–485. <https://doi.org/10.1016/j.electacta.2017.07.108>
- Nie S, Hao N, Zhang K, Xing C, Wang S (2020a) Cellulose nanofibrils-based thermally conductive composites for flexible electronics: a mini review. *Cellulose* 27:4173–4187. <https://doi.org/10.1007/s10570-020-03103-y>
- Nie S, Mo J, Zhang Y, Xiong C, Wang S (2020) Ultra-high thermal-conductive reduced graphene oxide welded cellulose nanofibrils network for efficient thermal management. *Carbohydr Polym* 250:116971. <https://doi.org/10.1016/j.carbpol.2020.116971>
- Pääkkönen T, Spiliopoulos P, Knuts A, Nieminen K, Johansson LS, Enqvist E, Kontturi E (2018) From vapour to gas: optimising cellulose degradation with gaseous HCl. *React Chem Eng* 3:312–318. <https://doi.org/10.1039/C7RE00215G>
- Pääkkönen T, Spiliopoulos P, Nonappa KKS, Penttilä P, Viljanen M, Svedström K, Kontturi E (2019) Sustainable high yield route to cellulose nanocrystals from bacterial

- cellulose. *ACS Sustain Chem Eng* 7:14384–14388. <https://doi.org/10.1021/acssuschemeng.9b04005>
- Phanthong P, Reubroycharoen P, Hao X, Xu G, Abudula A, Guan G et al (2018) Nanocellulose: Extraction and application. *Carbon Resour Convers* 1:32–43. <https://doi.org/10.1016/j.crccon.2018.05.004>
- Pottathara YB, Bobnar V, Grohens Y, Sabu T, Kargl R, Kokol V (2021) High dielectric thin films based on UV-reduced graphene oxide and Tempo-oxidized cellulose nanofibers. *Cellulose* 28:3069–3080. <https://doi.org/10.1007/s10570-021-03701-4>
- Putkonen M, Sippola P, Svärd L, Sajavaara T, Vartiainen J, Buchanan I, Forsström U, Simell P, Tammelin T (2017) Low-temperature atomic layer deposition of SiO<sub>2</sub>/Al<sub>2</sub>O<sub>3</sub> multilayer structures constructed on self-standing films of cellulose nanofibrils. *Phil Trans R Soc A* 376:20170037. <https://doi.org/10.1098/rsta.2017.0037>
- Sadasivuni KK, Ponnamma D, Ko HU, Kim HC, Zhai L, Kim J (2016) Flexible NO<sub>2</sub> sensors from renewable cellulose nanocrystals/iron oxide composites. *Sens Actuators B Chem* 233:633–638. <https://doi.org/10.1016/j.snb.2016.04.134>
- Sahu N, Parija B, Panigrahi S (2009) Fundamental understanding and modeling of spin coating process: A review. *Indian J Phys* 83:493–502. <https://doi.org/10.1007/s12648-009-0009-z>
- Singh T, Lehnen T, Leuning T, Sahu D, Mathur S (2014) Thickness dependence of optoelectronic properties in ALD grown ZnO thin films. *Appl Surf Sci* 289:27–32. <https://doi.org/10.1016/j.apsusc.2013.10.071>
- Spiliopoulos P, Spirk S, Pääkkönen T, Viljanen M, Svedström K, Pitkänen L, Awais M, Kontturi E (2021) Visualizing degradation of cellulose nanofibers by acid hydrolysis. *Biomacromol* 22:1399–1405. <https://doi.org/10.1021/acs.biomac.0c01625>
- Tynell T, Karppinen M (2014) Atomic layer deposition of ZnO: a review. *Semicond Sci Technol* 29:043001
- Tynell T, Giri A, Gaskins J, Hopkins PE, Mele P, Miyazaki K, Karppinen M (2014) Efficiently suppressed thermal conductivity in ZnO thin films via periodic introduction of organic layers. *J Mater Chem A* 2:12150–12152. <https://doi.org/10.1039/C4TA02381A>
- Uetani K, Hatori K (2017) Thermal conductivity analysis and applications of nanocellulose materials. *Sci Technol Adv Mater* 18:877–892. <https://doi.org/10.1080/14686996.2017.1390692>
- Vignaud G, Gibaud A (2019) REFLEX: a program for the analysis of specular X-ray and neutron reflectivity data. *J Appl Cryst* 52:201–213. <https://doi.org/10.1107/S1600576718018186>
- Wan C, Gu X, Dang F et al (2015) Flexible n-type thermoelectric materials by organic intercalation of layered transition metal dichalcogenide TiS<sub>2</sub>. *Nat Mater* 14:622–627. <https://doi.org/10.1038/nmat4251>
- Wan C, Tian R, Kondou M, Yang R, Zong P, Koumoto K (2017) Ultrahigh thermoelectric power factor in flexible hybrid inorganic-organic superlattice. *Nat Commun* 8:1–9. <https://doi.org/10.1038/s41467-017-01149-4>
- Weißl M, Rath T, Sattelkow J, Plank H, Eyley S, Thielemans W, Trimmel G, Spirk S (2019) Multi-layered nanoscale cellulose/CuInS<sub>2</sub> sandwich type thin films. *Carbohydr Polym* 203:219–227. <https://doi.org/10.1016/j.carbpol.2018.09.063>
- Wicklein B, Kocjan A et al (2015) Thermally insulating and fire-retardant lightweight anisotropic foams based on nanocellulose and graphene oxide. *Nat Nanotechnol* 10:277–283. <https://doi.org/10.1038/nnano.2014.248>
- Wyman CE, Decker SR, Himmel ME, Brady JW, Skopec CE, Viikari L (2005) Hydrolysis of cellulose and hemicellulose. *Polysaccharides: Struct diversity functional versatility* 1023–1062.
- Yang W, Zhang Y, Liu T, Huang R, Chai S, Chen F, Fu Q (2017) Completely green approach for the preparation of strong and highly conductive graphene composite film by using nanocellulose as dispersing agent and mechanical compression. *ACS Sustain Chem Eng* 5:9102–9113. <https://doi.org/10.1021/acssuschemeng.7b02012>
- Yousfi EB, Fouache J, Lincot D (2000) Study of atomic layer epitaxy of zinc oxide by in-situ quartz crystal microgravimetry. *Appl Surf Sci* 153:223–234. [https://doi.org/10.1016/S0169-4332\(99\)00330-X](https://doi.org/10.1016/S0169-4332(99)00330-X)
- Zhang K, Zhang Y, Yan D, Zhang C, Nie S (2018) Enzyme-assisted mechanical production of cellulose nanofibrils: thermal stability. *Cellulose* 25:5049–5061. <https://doi.org/10.1007/s10570-019-02694-5>
- Zhang K, Lu Y, Hao N, Nie S (2019) Enhanced thermal conductivity of cellulose nanofibril/ aluminum nitride hybrid films by surface modification of aluminum nitride. *Cellulose* 26:8669–8683. <https://doi.org/10.1007/s10570-019-02694-5>
- Zhang Y, Hao U, Lin X, Nie S (2020) Emerging challenges in the thermal management of cellulose nanofibril-based supercapacitors, lithium-ion batteries and solar cells: A review. *Carbohydr Polym* 234:115888. <https://doi.org/10.1016/j.carbpol.2020.115888>
- Zoubi WA, Yoon DK, Kim YGK, Young GK (2020) Fabrication of organic-inorganic hybrid materials on metal surface for optimizing electrochemical performance. *J Colloid Interface Sci* 573:31–44. <https://doi.org/10.1016/j.jcis.2020.03.117>
- Zu G, Shen J, Zou L, Wang F, Wang X, Zhang Y, Yao X (2016) Nanocellulose-derived highly porous carbon aerogels for supercapacitors. *Carbon* 99:203–211. <https://doi.org/10.1016/j.carbon.2015.11.079>